Thesis for the Degree of Licentiate of Engineering

VCSEL Techniques for Wavelength-Multiplexed Optical Interconnects

Mehdi Jahed

CHALMERS

Photonics Laboratory
Department of Microtechnology and Nanoscience
Chalmers University of Technology
Göteborg, Sweden, 2019

VCSEL Techniques for Wavelength-Multiplexed Optical Interconnects

Mehdi Jahed

Technical Report MC2 - 417
ISSN 1652-0769

Photonics Laboratory
Department of Microtechnology and Nanoscience
Chalmers University of Technology
SE–412 96 Göteborg
Sweden
Telephone: +46–(0)31–772 10 00

Printed by Chalmers Reproservice, Chalmers University of Technology
Göteborg, Sweden, 2019

VCSEL Techniques for Wavelength-Multiplexed Optical Interconnects

Mehdi Jahed
Photonics Laboratory
Department of Microtechnology and Nanoscience
Chalmers University of Technology

Abstract

The majority of global data communication is taking place within data centers where data is stored and processed and where the largest part of the power used for global networking is consumed. With the rapidly increasing use of Internet-based applications and services, data centers are equipped with a larger number of servers and switches requiring higher bandwidth connectivity. Optical interconnects (OIs) are used to provide the connectivity needed. Short-reach OIs are dominated by 850 nm GaAs-based vertical-cavity surface-emitting lasers (VCSELs) due to their low fabrication cost, low power consumption, high modulation speed, and circular output beam. With the need for even higher bandwidth connectivity, large efforts have been invested in the development of VCSEL-based OIs offering higher aggregate capacity. Until now, higher capacity has been achieved mostly through an increase of the lane rate by higher speed VCSELs and higher order modulation formats. Furthermore, spatial division multiplexing (SDM), using parallel fibers or multicore fibers, has proven effective for increasing the aggregate capacity. With these techniques, it is expected that the OI capacity will saturate at the $\sim$ 1 Tbit/s level.

Capacity beyond the limits of current technologies is expected by also exploring the wavelength dimension, referred to as wavelength division multiplexing (WDM). This calls for the development of high-speed VCSELs at multiple wavelengths. To also enable the very small footprint transceivers and high bandwidth density needed as transceivers move closer to the switch AISC, the multiple wavelength VCSELs should be in a monolithic array. This requires a VCSEL technology where the wavelength of individual VCSELs can be precisely set in a post-growth fabrication process. As an integration platform for multiplexing and fiber coupling we envision a photonic circuit on Si with Si_3N_4 waveguides and grating couplers for VCSEL integration. With such waveguides being single mode and the grating couplers being polarization sensitive, the VCSELs in the array should be single transverse and polarization mode, in addition to having a high modulation bandwidth.

In this thesis, an intra-cavity phase tuning technique, based on an Ar ion-beam etching process with sub-nm precision, is demonstrated for setting the resonance wavelength of VCSEL resonators with <2 nm precision in the wavelength range 1040-1070 nm. Single transverse and polarization mode VCSELs with a record output power of 6 mW are also demonstrated. Suppression of higher order transverse modes and the orthogonal polarization state is achieved by etching a shallow mode filter in the surface of the VCSEL.

Keywords: vertical-cavity surface-emitting laser, optical interconnect, wavelength-multiplexing, silicon photonic integration, transverse and polarization mode filter, distributed Bragg reflector.

List of papers

This thesis is based on the following appended papers:

[A] **M. Jahed**, J. S. Gustavsson, A. Larsson, "Precise setting of micro-cavity resonance wavelength by dry etching", *Journal of Vacuum Science and Technology B*, vol. 37, 031217 (2019),
https://doi.org/10.1116/1.5092192

[B] E. Haglund, **M. Jahed**, J. S. Gustavsson, A. Larsson, J. Goyvaerts, R. Baets, G. Roelkens, M. Rensing, P. O'Brien, "High-power single transverse and polarization mode VCSEL for silicon photonics integration", *Optics Express*, vol. 27, pp. 18892-18899 (2019),
https://doi.org/10.1364/OE.27.018892

Related conference publication and presentation by the author:

[C] **M. Jahed**, J. S. Gustavsson, A. Larsson, "Precise setting of VCSEL resonance wavelength by dry etching", *21st International Vacuum Congress (IVC-21)*, Jul. 1-5, 2019.

Acknowledgement

Many people have supported me during this work and deserve for my gratitude. First of all, I would like to thank my supervisor and examiner Prof. Anders Larsson for giving me the opportunity to work in this exciting field, his excellent support and fruitful discussions. I am grateful to my assistant supervisor Johan Gustavsson for his simulations, fruitful discussions and support. I would like to thank Emanuel P. Haglund for an excellent introduction to VCSEL fabrication, measurement techniques and sharing his knowledge with me. Erik Haglund deserves my gratitude for always sharing his vast knowledge in VCSEL fabrication and measurement. I also would like to thank Ewa and Alexander for always being there for discussion, characterization and fabrication.

I am honored to be a member of Photonics Lab and have so many wonderful friends and colleagues who make such a nice environment to work and many memorable moments. Especially, I am thankful to Elham for our friendship and supporting me in my personal life. Thank you, Jeanette, for being such an excellent and nice secretary. I also would like to thank Nanofabrication Laboratory staff for their excellent support, sharing knowledge and keeping the tools at the best performance.

Last, but definitely not least I would like to express my gratitude from deepest part of my heart to my beloved wife and family. My love, Sahar, you mean everything to me.

This work is financially supported by the Swedish Research Council (project iTRAN, 2016-06077), the Swedish Foundation for Strategic Research (project MuTOI, SE13-0014), and the European Union's Horizon 2020 Research and Innovation Program (project PIX4life, 688519). IQE Europe and JENOPTIK AG are acknowledged for supplying the epitaxial VCSEL materials.

Mehdi Jahed

Göteborg
September 2019

Contents

Abstract iii

List of papers v

Acknowledgement vii

List of abbreviations xi

1 Introduction 1
- 1.1 Data center architecture . . . 1
- 1.2 Toward higher capacity data center connectivity . . . 3
- 1.3 VCSEL-based optical interconnects . . . 4

2 Wavelength multiplexed optical interconnects 5
- 2.1 Dense and coarse WDM . . . 5
- 2.2 VCSEL-based WDM interconnects . . . 6
  - 2.2.1 Monolithic multi-wavelength VCSEL arrays, state-of-the-art . . . 6
  - 2.2.2 Integrated CWDM transceivers . . . 7
  - 2.2.3 VCSEL requirements . . . 8

3 Vertical-cavity surface-emitting lasers 9
- 3.1 Concept and basic performance . . . 10
- 3.2 VCSEL dynamics . . . 11
- 3.3 VCSELs for CWDM transmitter integration . . . 12
  - 3.3.1 Wavelength setting . . . 13
  - 3.3.2 Transverse and polarization mode control . . . 14

4 VCSEL fabrication 15
- 4.1 Metallization and selective oxidation . . . 15
- 4.2 Etching for intra-cavity phase tuning . . . 16
- 4.3 Dielectric DBR deposition . . . 16
- 4.4 Mode filter integration . . . 17

5 Future outlook 19

6 Summary of papers 21

Appended papers A–B **29**

List of Abbreviations

AFM	atomic force microscopy
BCB	benzocyclobutene
BW	bandwidth
CMOS	complementary metal-oxide-semiconductor
CWDM	coarse wavelength division multiplexing
DBR	distributed Bragg reflector
DEMUX	demultiplexer
DMT	discrete multitone
DWDM	dense wavelength division multiplexing
FEC	forward error correction
LED	light emitting diode
MBE	molecular beam epitaxy
MCF	multicore fiber
MMF	multimode fiber
MOCVD	metal-organic chemical-vapor deposition
MQW	multiple quantum well
MUX	multiplexer
NRZ	non-return-to-zero
OI	optical interconnect
OOK	on-off keying
PAM-4	4-level pulse amplitude modulation
PD	photodetector
PIC	photonic integrated circuit
QW	quantum well
SDM	spatial division multiplexing
SiP	silicon photonics
SMF	single-mode fiber
SOI	silicon-on-insulator
SPM	scanning probe microscopy
ToR	top-of-rack
VCSEL	vertical-cavity surface-emitting laser
WDM	wavelength division multiplexing

Chapter 1

Introduction

At the time of writing this thesis, 56.8% of the world population use the Internet. The world population of Internet users in 2019 has grown by 100% compared to 2000 and reached 4,383,810,342 in March 2019. The maximum growth (10.815%) was in Africa and 50.1% of the Internet users live in Asia [1]. Every day we use the Internet to connect with friends and family, stream music and movies, share ideas and knowledge, search for information, shop online, etc. It is difficult to imagine the world without the Internet.

Two key components of the Internet infrastructure are optical fiber cables and data centers. Vast amounts of data are transmitted through these cables across the world while data is being processed, stored, and accessed in data centers. With increasing use of Internet-based applications and cloud computing, the number of the data centers and their size increase rapidly. Our computers, smartphones, and tablets are mainly used as terminals where we access information, while data storage and processing is located in the data centers. The number of hyperscale data centers was 259 in 2015 and is predicted to be 485 in 2020 [2]. The largest data center in the world had a size of 100,000 square meter (equivalent to 12 FIFA standard football fields) in 2015 [3] and 10.7 million square foot in 2019 [4] (nearly 120 football fields). This up-scaling means that present and future data centers, as well as supercomputers, need an internal communication network with huge capacity. Both longer reach (up to 2 km) and shorter reach (meter's) OIs are needed when data centers increase in size and when OIs are increasingly used in the server racks. GaAs-based vertical-cavity surface-emitting lasers (VCSELs), offering low cost, low power consumption, small footprint, high modulation speed at low current, and excellent reliability, are well-suited for short reach OIs in particular [5, 6].

1.1 Data center architecture

Data centers, either room-scale or hyperscale, are made of cabinets of servers. Since the number of hyperscale data centers is increasing and they are the main hubs for

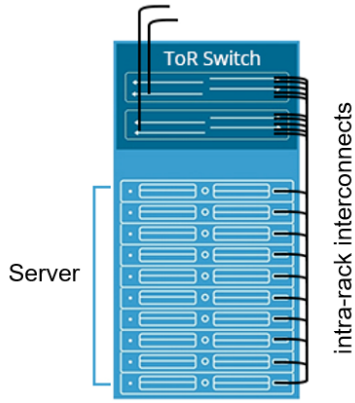

Figure 1.1: A schematic view of a rack of servers. Each server connects to the ToR switch via intra-rack interconnects [7].

the global data traffic, in this section, the architecture of a hyperscale data center is introduced. In the hyperscale data center, there are numerous racks of stacked servers and storage units clustered in pods. Each rack contains multiple servers or storage units. A top-of-rack (ToR) switch interconnects all units within the rack. The ToR switch, like a gigabit Ethernet switch, can be put anywhere in the rack, not just limited to the top. However, engineers prefer to have the ToR at the top for easier accessibility and cleaner cable management, figure 1.1. Moreover, the ToRs are connected using additional layers of network switches. The way swicthes are connected to each other is called topology. In a hyperscale data center, careful consideration of topology is necessary due to network throughput, latency, congestion, and packet loss [8, 9]. Furthermore, the up-scale topology needs to support a large inter-node communication bandwidth. The fat-tree topology was proposed for fulfilling these requirements [10].

A simplified view of a fat-tree topology is shown in figure 1.2. The motivation behind the fat-tree topology is achieving maximum bisection bandwidth in the network, which requires spreading outgoing traffic from any given pod as evenly as possible among the core switches. The fat-tree topology provides large bisectional bandwidth, economical scalability, low power consumption, and backward compatibility in large data centers [9–12].

Today's interconnects employ optical fibers instead of copper cables. They provide higher data rates with large bandwidth, minimum attenuation, and low power consumption [13], and there is no crosstalk or any electromagnetic interference [14,15]. The most common OI consists of a GaAs-based VCSEL operating at 850 nm with a multi-mode fiber (MMF) [11].

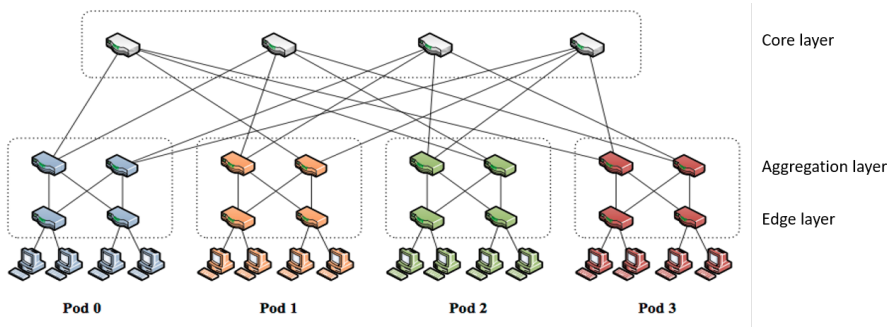

Figure 1.2: Simplified view of a fat-tree topology. Core layer switches are on top and connect to each server in pods via aggregation layer and edge layer switches [10].

1.2 Toward higher capacity data center connectivity

The 850 nm GaAs-based VCSEL technology is used in 95% of all optical networking applications with reach <1000 m [16]. In a data center, 850 nm VCSELs are used as the light source in short-reach OIs (intra-rack and lower level network). However, as the throughput of servers and switches increase, the increasing number of transceivers in a limit space presents a formidable challenge. Hence, there is a great need for higher capacity and higher bandwidth density OI transceivers [17].

Large efforts have been invested in the development of higher aggregate capacity OIs. On-off-keying, non-return-to-zero (OOK-NRZ) data transmission up to 57 Gbit/s at 25°C and 50 Gbit/s at 85°C, without equalization or forward-error-correction (FEC), has been achieved using 850 nm VCSELs [18]. With transmitter and receiver equalization, error-free data rates >70 Gbit/s have been demonstrated [19]. More recently, 1060 nm single and multimode VCSELs (GaAs-based) were investigated for extending the reach of VCSEL-based OIs [20]. Extended reach is enabled by the lower fiber chromatic dispersion and attenuation at longer wavelengths [21]. To further increase capacity, higher order modulation formats are used. The PAM-4 format is of primary interest because of low power consumption and low complexity. PAM-4 with transmitter equalization and pulse shaping has enabled error-free (no FEC) 100 Gbit/s transmission over 100 m MMF at 850 nm [22]. Further improvements of aggregate capacity, and bandwidth density, may come from the use of multiple cores per fiber (spatial division multiplexing, SDM) or multiple wavelengths per fiber (wavelength division multiplexing, WDM). A multicore fiber interconnect with a single fiber capacity of 240 Gbit/s has been demonstrated using a 6-core fiber and a 6-element VCSEL array [23]. Coarse WDM with 4 channels and 30 nm channel spacing (850, 880, 910, and 940 nm), known as SWDM4, is being implemented [24] and has demonstrated up to 400 Gbit/s (4x100 Gbit/s) single fiber capacity [25]. With WDM being the most promising and scalable approach for higher aggregate capacity and higher bandwidth density, increasing the number of

wavelengths per fiber from 4 to 8 and beyond is considered to increase the capacity on a single fiber to ∼1 Tbit/s and the aggregate capacity on multiple fibers to ∼10 Tbit/s [26].

1.3 VCSEL-based optical interconnects

A schematic of a VCSEL-based single-channel OI is shown in figure 1.3. It is composed of a transmitter, an optical fiber, and a receiver. The VCSEL-based transmitter consists of a VCSEL, which is directly modulated by a driver to convert the electrical input signal to an optical signal which is transmitted along the optical fiber. At the receiver, the received signal is converted back to the electrical domain by a photodetector and a transimpedance amplifier and subsequently amplified to a sufficient level.

Short-reach (<300 m) OI transmitters employ predominantly 850 nm GaAs-based VCSELs [5]. For longer reach, VCSELs emitting at longer wavelengths can be employed. The VCSEL emission wavelength depends on the semiconductor compounds used in the VCSEL structure. In the GaAs-based VCSEL, with AlGaAs compounds in the mirrors and InGaAs compounds in the active region, the wavelength can be extended to ∼1100 nm [27]. For longer wavelength VCSELs at 1310 and 1550 nm, InP-based compounds are used. However, while optical fiber performance is optimum at 1310 nm (minimum chromatic dispersion) and 1550 nm (minimum attenuation), InP-based VCSELs suffer from higher threshold currents due to a higher non-radiative recombination rate [28] and more complex mirror designs due to the small refractive index contrast offered by the InP-based compounds.

The optical fiber link provides broad bandwidth transmission, low cost, light weight, high security, and immunity to electromagnetic interference compared to the copper cables. Its attenuation is low but wavelength dependent, 2 dB/km at 850 nm and 0.2 dB/km nm at 1550 nm [21]. The MMF used in OIs is more expensive than the single-mode fiber (SMF) due to its complex refractive index profile [29] but offers relaxed alignment tolerance to the light source because of its large core size. Single-mode technology (SMF and single-mode VCSEL) can be used to extend reach but it needs more critical alignment and therefore increases assembly and packaging cost.

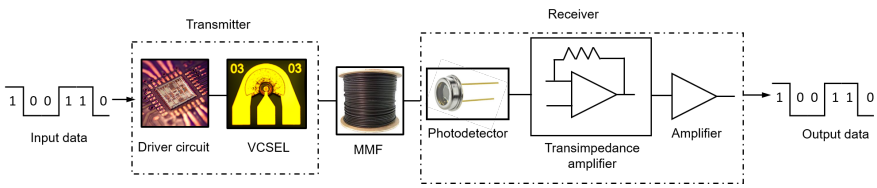

Figure 1.3: Single-channel VCSEL-based OI.

Chapter 2

Wavelength multiplexed optical interconnects

The performance of a data center has become largely limited by the capacity and efficiency of the networks used to interconnect servers, storage units, and switches. Future data centers with very large scale and bandwidth will need networks with very high aggregate capacity (a thousand times higher than today's maximum capacity). In addition to higher speed VCSELs (with baud rates of 50 and 100 Gbaud/s) together with higher order modulation formats (PAM-4, PAM-8, DMT, duobinary $\cdots$) for higher lane rates, multiplexing is needed for very high aggregate capacity. Spatial division multiplexing (SDM) employs parallel fibers or a multicore fiber (MCF) to transmit a channel per fiber core and therefore multiplies the net capacity. Until now, higher OI capacity has been achieved predominantly through an increase of the lane rate and through the use of parallel fibers [23]. Future large-scale data centers will require multi-Tbit/s interconnect capacity and major improvements of bandwidth density. However, current OI technologies are expected to saturate at the $\sim$1 Tbit/s level. Wavelength division multiplexing (WDM), with multiple channels at different wavelengths on a single fiber core, is considered the solution for reaching multi-Tbit/s capacity.

2.1 Dense and coarse WDM

In a WDM system, see figure 2.1, several signals at different wavelengths, emitted by different lasers, are combined in a multiplexer (MUX) and transmitted together through a single fiber with a single core. At the receiver, they are split by a demultiplexer (DEMUX) and detected by an array of photodetectors (PDs). Thus, interconnect capacity can be increased without increasing the amount of optical fibers [30]. This also improves the bandwidth density. WDM systems are classified according to the spectral density of multiplexed channels. VCSEL-based SWDM4 OIs, with direct modulation and direct detection, use a channel spacing of 30 nm and four discrete VCSELs emitting at different wavelengths. This is referred to as coarse WDM

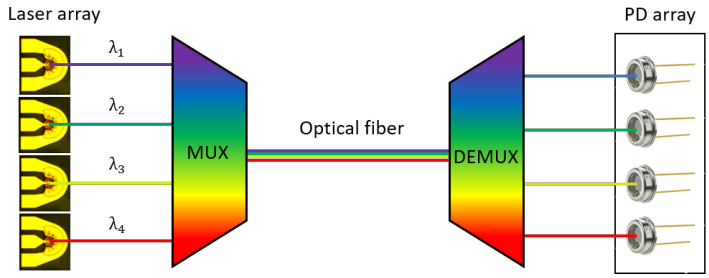

Figure 2.1: Four-channel WDM system.

(CWDM). The large channel spacing simplifies system implementation and accommodates the drift in wavelength with temperature (∼4 nm from 25 to 70°C for a GaAs-based VCSEL at ∼1000 nm). In long haul optical communication systems, dense WDM (DWDM) is used. Here, the channel spacing is much smaller and the number of channels is much larger, e.g. 80 channels with 50 GHz spacing. This requires the use of coherent techniques for encoding and decoding of data on the optical carriers.

2.2 VCSEL-based WDM interconnects

In data center servers and switches, as well as the data processing and storage equipment used in supercomputers, there is a large number of OI transceivers in a limited space. Therefore, bandwidth density, quantified by the Gbit/s/mm^2 figure of merit, is an important measure [31]. Any form of multiplexing (SDM or WDM) of the interconnect channels, which could improve bandwidth density, is therefore of interest. The maximum achievable capacity of VCSEL-based OIs using SDM is considered to be at the ∼1 Tbit/s level. However, future data centers will need at least an order of magnitude higher capacity and this can potentially be provided by WDM. The use of discrete VCSELs emitting at different wavelengths (e.g. SWDM4) can be used to build WDM transmitters but the use of discrete components increases the footprint and limits the bandwidth density. With monolithic multi-wavelength arrays of VCSELs, both high aggregate capacity and high bandwidth density can be achieved [30].

2.2.1 Monolithic multi-wavelength VCSEL arrays, state-of-the-art

The resonance wavelength of a VCSEL is set by the phase of the reflections from the distributed Bragg reflectors (DBRs) and the propagation phase delay in the cavity separating the DBRs. The latter is controlled by the optical length of the cavity. Therefore, both reflection phases and cavity length are parameters that can be used to set the wavelength of VCSELs in a multi-wavelength VCSEL array.

Since the early 1990's, different techniques for fabricating monolithic multi-wavelength

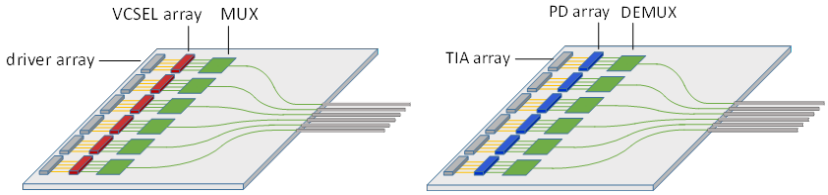

Figure 2.2: Left: SiP transmitter with flip-chip mounted multi-wavelength VCSEL arrays and multi-channel drivers and integrated MUXs. Right: SiP receiver with flip-chip mounted photodetector (PD) arrays and multi-channel transimpedance amplifiers (TIAs) and integrated DEMUXs.

VCSEL arrays have been explored. Non-uniform [32] and non-planar [33] epitaxial growth were used to induce a variation in cavity length, and therefore wavelength, over the wafer. However, VCSEL designs and fabrication techniques that allow for post-growth wavelength setting are preferred for precisely controlling the emission wavelength of VCSELs at specific locations on the wafer. Among these techniques, non-planar bonding to control the cavity length of wafer bonded VCSEL [34], selective oxidation for modifying the cavity length [35, 36], replacement of the top-DBR by a high-contrast grating to control the reflection phase by the grating parameters [37], the use of an intra-DBR phase tuning layer for controlling the DBR reflection phase [38–42], and the use of an intra-cavity phase tuning layer for controlling the cavity length [43, 44] have been explored. The generation of a 400 Gb/s line rate signal, which consists of four WDM channels with a 100 GHz channel spacing and each channel carrying a 100 Gb/s PDM-4PAM signal was demonstrated by using a monolithic 2×4 directly modulated 1.55 μm single mode VCSEL array [45].

2.2.2 Integrated CWDM transceivers

The construction of compact CWDM transmitters with small footprint and high bandwidth density requires an integration platform on which multi-wavelength VCSEL arrays and multi-channel drivers can be mounted and the different wavelength channels can be multiplexed and coupled to a single fiber. A similar integration platform is need for the receiver, with a demultiplexer and arrays of photodetectors and transimpedance amplifiers. We envision using a CMOS compatible silicon photonics (SiP) integration platform for this purpose (Fig. 2.2). Such platforms, with silicon-on-insulator (SOI) waveguides for wavelengths >1100 nm and silicon nitride (SiN) waveguides for wavelengths <1100 nm, are available with low waveguide loss and low loss MUXs and DEMUXs [46].

Flip-chip integration of VCSELs over grating couplers (Fig. 2.3) enable independent optimization of VCSEL performance. The tilt eliminates optical feedback to the VCSEL and facilitates unidirectional coupling to the waveguide without the need of e.g. a slanted grating coupler.

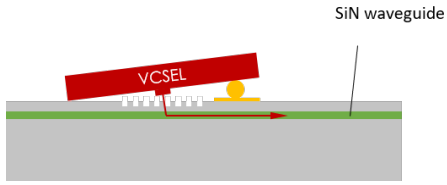

Figure 2.3: Flip-chip integration of a VCSEL at an angle over a grating coupler in the SiN waveguide.

2.2.3 VCSEL requirements

While flip-chip integration of a VCSEL over a grating coupler in the SiP integrated circuit offers certain advantages [47,48] it is also demanding for the modal properties of the VCSEL, in addition to the wavelength having to be precisely controlled. Since the grating coupler is polarization sensitive and with the waveguides being single-mode, the VCSEL has to be single (fundamental) transverse mode with a stable and linear polarization state. In addition, to overcome optical losses in the different parts of the SiP circuits (grating couplers, multiplexers, demultiplexers, and fiber couplers), high output power from the VCSEL is required. To fabricate a single transverse mode oxide-confined VCSEL, different approaches are available. Since number of transverse modes is controlled by the size of the oxide aperture, a small aperture ($< \sim 3\ \mu$m) results in a single transverse mode operation. However, small aperture VCSELs have high resistance and limited output power. Higher power can be achieved with a larger aperture (lower resistance) and a mode filter etched in the surface of the VCSEL. With a proper size of the mode filter with respect to the aperture, higher order transverse modes can be suppressed and single-mode emission with >30 dB suppression of higher order modes can be achieved [49]. With a grating in the mode filter (Fig. 2.4), the polarization can also be pinned for >20 dB suppression of the orthogonal polarization mode [50]. If the grating pitch is sub-wavelength, beam degradation due to diffraction is avoided [51].

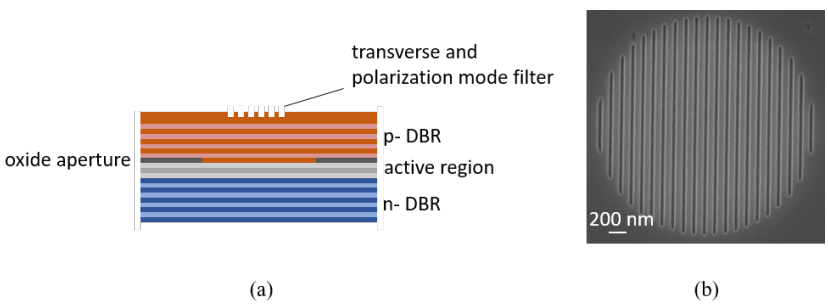

Figure 2.4: (a) An oxide-confined VCSEL with a sub-wavelength grating mode filter etched into the surface. (b) Top view of the mode filter.

Chapter 3

Vertical-cavity surface-emitting lasers

The vertical-cavity surface-emitting laser (VCSEL) is a semiconductor laser which emits light from the surface, Figure 3.1.a. The cavity consists an un-doped active region sandwiched between two p- and n-doped highly reflective (∼99%)distributed Bragg reflectors (DBRs). Optical gain is provided when the pn-junction is forward biased. In contrast to the VCSEL, an edge-emitting Fabry Perot (FP) laser, the simplest type of semiconductor lasers, has a horizontal resonator with cleaved semiconductor-air facets acting as the mirrors, Figure 3.1.b. Therefore, the wafer has to be cleaved before testing. The VCSEL, on the other hand, can be tested on-wafer during production and easily integrated into 2D arrays.

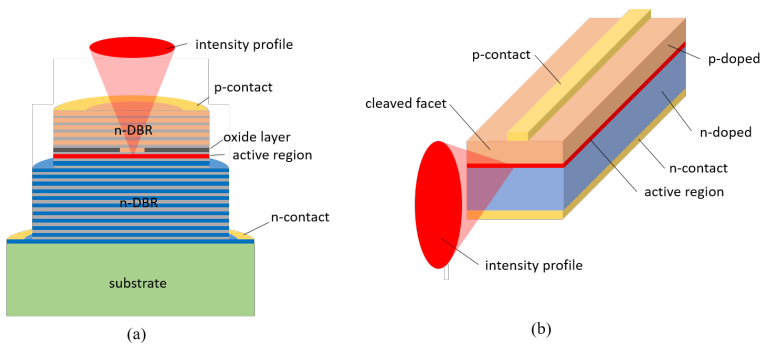

Figure 3.1: Geometry and optical output of (a) an oxide-confined VCSEL and (b) an edge emitting FP laser.

3.1 Concept and basic performance

In a semiconductor laser, the gain medium is composed of a thin undoped (intrinsic) direct bandgap layer (active region) sandwiched between p- and n-doped layers with higher bandgap and that form a pin junction. When applying a forward bias to the pin junction, electrons and holes are injected and accumulate in the active region where radiative transitions and recombination occur. For small currents, the majority of the radiative transition is spontaneous emission. Increasing the bias current increases the optical gain and at a certain current (threshold current) it balances the cavity losses (internal loss and mirror losses) and lasing starts. The material gain at the threshold (g_{th}) is defined as:

$$g_{th} = \frac{1}{\Gamma}[\alpha_i + \alpha_m] = \frac{1}{\Gamma}[\alpha_i + \frac{1}{2L}\ln(\frac{1}{R_1 R_2})]. \tag{3.1}$$

where Γ is the optical confinement factor, which defines the overlap between the active region and the optical field. α_i and α_m are internal and mirror loss, respectively. In a VCSEL, L is the effective cavity length and R_1 and R_2 define the DBR reflectivities. The threshold current can be calculated from the threshold gain and the gain and recombination parameters. Apart from the gain condition, for lasing to occur, the phase of the optical field must repeat itself after one round-trip inside the resonator (resonance condition):

$$exp(-j\frac{2\pi}{\frac{\lambda_0}{n_{eff}}}.2L) = 1 \rightarrow \lambda_0 = \frac{2Ln_{eff}}{m}, \tag{3.2}$$

where λ_0 defines the free space resonance wavelengths, n_{eff} is the refractive index of the lasing mode, and m is an integer that defines a longitudinal mode.

In a VCSEL with a thin active region and a short cavity, optical feedback and vertical confinement is provided by highly reflective top and bottom DBRs. The effective cavity length is only a few wavelengths and therefore the longitudinal mode spacing is large. Thus, only one longitudinal mode is within the gain bandwidth. In a GaAs-based oxide-confined VCSEL, an oxide aperture (a partly oxidized high-Al content layer) is placed close to the active region to confine the optical fields and the injection current in the transverse plane. The strength of the transverse optical confinement depends on the size of the aperture, the thickness of the oxidized layer, and its vertical position relative the optical fields. Depending on the strength, the VCSEL can support one or multiple transverse modes (single or multimode VCSEL). A single-mode VCSEL requires a small aperture diameter.

Since light in a VCSEL propagates perpendicular to the thin active region, the round trip gain is low and highly reflective DBRs are required for low resonator loss. A DBR is a stack of multiple layers with alternating refractive indices. Each layer is quarter wavelength thick and reflections from different interfaces of the DBR interfere constructively to generate a high DBR reflectivity. The number of layer pairs required depends on the refractive index contrast. For instance, a semiconductor DBR with different Al-content AlGaAs layers has a low index contrast and needs 20-30 pairs, while a dielectric DBR typically requires less than 10 pairs to reach >99% reflectivity. Because of the vertical geometry of the VCSEL resonator, the round-trip optical gain is limited by the thin active region. To achieve sufficient gain for lasing, multiple

quantum wells (QWs) are used in the active region since for equal thickness, QWs provide higher gain than bulk material [52].

3.2 VCSEL dynamics

Data centers are dominated by VCSEL-based OIs and their capacity depends on the VCSEL dynamics. To encode data on the light emitted by the VCSEL, its intensity is directly modulated by the current. The VCSEL must be fast enough to react to changes in the current at the data rate considered. Since electron-hole recombination is associated with a certain lifetime (the differential carrier lifetime) and since it takes some time for generated photons to escape from the resonator (the photon lifetime), the VCSEL cannot be modulated infinitely fast. Therefore, a proper and intelligent design is needed for a high modulation bandwidth.

The dynamic properties of a VCSEL, like any other directly modulated semiconductor laser, are described by the resonant interaction between injected carriers in the active region and photons in the lasing modes of the resonator. This interaction is described by rate equations for the carrier and photon densities [52]:

$$\frac{dN}{dt} = \frac{\eta_i I}{qV_a} - \left(AN + BN^2 + CN^3\right) - v_g G S_m \tag{3.3}$$

$$\frac{dS_m}{dt} = \Gamma v_g G S_m - \frac{S_m}{\tau_p} + \Gamma \beta B N^2, \tag{3.4}$$

where N is the excess carrier density in the active region with volume V_a, η_i the internal quantum efficiency, I the injection current, and q the elementary charge. A, B and Care the Shockly-Read-Hall, the radiative, and the Auger recombination coefficient, respectively. v_g is the group velocity, G the active region gain per unit length, S_m the photon density in the active region for mode m, Γ the longitudinal optical confinement factor, τ_p the photon lifetime, and β the fraction of the spontaneous emission that enters the lasing mode. The subscript m shows that a separate rate equation for the photon density of each transverse mode is needed. However, in an oxide-confined VCSEL where the transverse optical fields are strongly overlapping, a single rate equation for the photon density is sufficient for capturing the most important aspects of VCSEL dynamics [53]. At high photon densities, gain compression due to nonlinear effects such as spectral hole burning and carrier heating [54] occur, and this can be accounted for by a photon density dependent optical gain:

$$G = \frac{g(N)}{1 + \epsilon S}. \tag{3.5}$$

where g and ϵ are the uncompressed gain and gain compression factor, respectively. Equations 3.3 and 3.4 are coupled differential equations and have to be solved numerically under arbitrary variations of the injection current. However, under small-signal modulation and using a single rate equation for the photon density, an analytical solution can be derived which yields a transfer function $H_i(f)$ for the intrinsic small-signal modulation response:

$$H_i(f) = \text{const} \cdot \frac{f_r^2}{f_r^2 - f^2 + j\frac{f}{2\pi}\gamma}. \tag{3.6}$$

with[57]:

$$f_r \approx \frac{1}{2\pi}\sqrt{\frac{v_g g_0 S}{\tau_p\,(1+\varepsilon S)}}, \tag{3.7}$$

and:

$$\gamma \approx K f_r^2 + \gamma_0, \qquad \text{with} \qquad K = 4\pi^2\left[\tau_p + \frac{\varepsilon}{v_g g_0}\right], \tag{3.8}$$

where f_r is the resonance frequency, γ the damping factor, g_0 the nominal differential gain, γ_0 the damping offset, and K is referred to as the K-factor.

The modulation bandwidth, f_3dB, is defined as the frequency at which the response is half of its low frequency value and the intrinsic bandwidth is ruled by the equation 3.8, since damping increases with current. A high resonance frequency, favored by a high photon density, a short photon lifetime, and high differential gain, is still needed for high modulation speed. The photon density and lifetime are to a large extent controlled by the reflectivity of the DBR through which light is coupled out (usually the top-DBR) and a high differential gain is provided by strained and deep QWs. The increase of the resonance frequency with current is quantified by the D-factor:

$$f_r = D \cdot \sqrt{I - I_{th}}, \qquad \text{with} \quad D = \frac{1}{2\pi}\sqrt{\frac{\eta_i \Gamma v_g}{qV_a} \cdot g_0}, \tag{3.9}$$

where I and I_{th} are the bias and threshold currents, respectively.

At high internal VCSEL temperature, caused by a high ambient temperature and/or current-induced self-heating, thermal effects limit the bandwidth by reducing the differential gain and increasing the leakage of carriers from the MQWs. At high modulation frequencies, electrical parasitics shunt the modulation current past the active region which reduces the modulation response. As a result, a VCSEL design with low electrical resistance, low capacitance, low heat generation, and low thermal impedance is needed for a high modulation bandwidth. The DBR resistance can be reduced by graded composition interfaces and modulation doping and by using an intra-cavity contact design [55]. The parasitic capacitance across the oxide layer can be reduced by adding extra oxide layers [56, 57]. Lower thermal impedance can be achieved by employing binary alloys in the DBR [58].

3.3 VCSELs for CWDM transmitter integration

In addition to a high modulation speed, there are three main requirements on a VCSEL for a monolithic multi-wavelength VCSEL array and its integration on a SiP integration platform for multiplexing (Fig. 2.2):

1. The wavelength should be precisely set
2. The VCSEL has to be single transverse mode with sufficient suppression

of higher order modes
3. Its polarization has to be linear and stable under variations of current and temperature

In this work, an intra-cavity phase tuning technique has been developed for precise wavelength setting. Intra-cavity phase tuning is a technique where the cavity length, and therefore the emission wavelength, of a VCSEL with an epitaxial bottom-DBR, active region, and current injection layer is modified before the deposition of a dielectric top-DBR. The cavity length can be changed by thinning either the semiconductor current injection layer above the active region [44] or an additional dielectric layer above the current injection layer [43] before top-DBR deposition. While intra-cavity phase tuning is most effective in controlling the resonance wavelength, it requires precise etching or deposition for accurate wavelength control. To achieve a single transverse mode with linear polarization and a high output power, the use of a mode filter etched into the surface of a VCSEL has been explored. The target wavelength range for the multi-wavelength VCSEL arrays is 1040-1070 nm and is motivated by opportunities for 1) developing high-performance single-mode VCSELs at these wavelengths [59], and 2) multiplexing in a SiN photonic integrated circuit on silicon with flip-chip integrated multi-wavelength VCSEL arrays [47] and low-voltage multi-channel drivers to form compact, high-efficiency, and high-capacity CWDM transmitters. The work on wavelength setting has used VCSEL structures designed for this wavelength range while the work on transverse and polarization mode control has used an 850 nm VCSEL design. The intention is to transfer the techniques for mode and polarization control to the VCSEL designs in the 1040-1070 nm range.

3.3.1 Wavelength setting

Intra-cavity phase tuning by thinning of the intra-cavity current injection layer before the top-dielectric DBR deposition has been used for wavelength setting. The work and results are reported in the appended Paper A. To thin the current injection layer, an Ar ion-beam etching process was used. Ar ion-beam etching is inherently a pure physical etch process and provides sub-nanometer precision in etch depth at a slow etch rate ($\sim$0.5 Å/s with 3 mA ion-beam current). As a result of etching, the cavity becomes shorter and consequently the resonance wavelength is blue-shifted. The etched surface is as smooth as the unetched. This is essential for high performance VCSELs since a rough surface would cause optical scattering loss, which would degrade performance (increase the threshold current and reduce the slope efficiency) because of the high optical field intensity at the semiconductor-dielectric interface close to the center of the resonator.

To form the full resonator, 6 pairs of SiO_2/TiO_2 with quarter-wavelength thick layers were sputtered on the etched surface to build the top-DBR. Deviations in thickness from a quarter-wavelength (ideally 182 and 116 nm, respectively, at the center wavelength of 1055 nm) lead to a change in the reflection phase and therefore in the resonance wavelength. Errors in the first dielectric DBR pair have the largest impact, while errors in pairs further away from the cavity have less impact. A precision in wavelength setting $<$2 nm is demonstrated.

3.3.2 Transverse and polarization mode control

A GaAs-based oxide-confined VCSEL with a relatively large oxide aperture, 5 μm, was used to provide high output power and low resistance. Since the oxide aperture is large, the VCSEL supports multiple transverse modes. To select the fundamental mode and pin the polarization, a transverse and polarization mode filter was used. The work and results are reported in the appended Paper B. The mode filter is a sub-wavelength grating etched in an area with a diameter less than the diameter of the oxide aperture, 3 μm. Before etching, the topmost layer optical thickness is a half wavelength which results in an anti-phase reflection at the surface that lowers the top-DBR reflectivity. After etching a mode filter to an effective depth of a quarter-wavelength, the reflectivity of the top-DBR becomes higher in the etched area. This spatially dependent reflectivity is used for transverse mode selectivity [60]. The sub-wavelength grating acts as a polarization dependent effective index medium. Therefore, the effective index for light polarized parallel and perpendicular to the grating lines is different and results in polarization selectivity [60]. Thus, the spatial extent of the mode filter controls the transverse mode selectivity while the orientation of the grating lines provides polarization mode selectivity. The sub-wavelength grating pitch, in contrast to a pitch larger than the wavelength, also avoids excessive optical loss and beam degradation due to diffraction. A record high output power of 6 mW was achieved with >30 dB suppression of higher order transverse modes and >20 dB suppression of the orthogonal polarization mode.

Chapter 4

VCSEL fabrication

The epitaxial VCSEL structures used in this work were grown using the metal-organic chemical-vapor deposition (MOCVD) technique and provided by IQE Europe Ltd. and JENOPTIK AG. MOCVD provides a good compromise between growth rate and control of layer thickness, composition, and doping. III-metals (Al, Ga, In) are transported into a reactor using gaseous organic compounds. They react with arsine (AsH_3) and adsorb on the heated substrate to form III-As epitaxial films. Introducing Si or C to the reactor results in n-type or p-type doping. After epitaxial growth, several processing steps are needed for the work in this thesis and for the fabrication of multi-wavelength VCSEL arrays. In this chapter, some of the main steps are discussed.

4.1 Metallization and selective oxidation

To be able to inject or extract current to and from any optoelectronic device with low resistance, ohmic contacts are needed. Metal thin films are usually deposited by electron beam evaporation, in which metal vapors are generated when a high-energy electron beam hits the metal source and are deposited on the sample. The deposition rate is accurately controlled by monitoring the mechanical resonance frequency of a crystal. The resonance frequency decreases with increasing film thickness. This evaporation technique was used to deposit Ti/Pt/Au p-contacts and Ni/Ge/Au n-contacts. Depositing the p-contact on a highly p-doped GaAs layer results in an ohmic contact with low resistivity. On the other hand, the n-contact deposited on highly n-doped GaAs requires annealing at 380°C for 1 minute for ohmic behavior with low resistivity.

In an oxide-confined VCSEL, the oxide aperture is formed by selective wet oxidation of a high-Al content AlGaAs layer by subjecting the etched mesa sidewall to hot water vapor at 420°C. A nitrogen bubbler is used to carry water vapor from a water container held at 95-97°C to the oxidation furnace. Using an array of infrared LEDs and a microscope with a CCD camera enables in-situ observation of the wet oxidation. The oxide aperture can be distinguished by the difference in reflectivity

between oxidized and non-oxidized areas. The oxidation rate is highly dependent on the furnace temperature and the Al concentration with even a small temperature gradient across the sample leading to large differences in oxidation rate. Since our furnace temperature is not uniform, the chip was turned 180 degrees half-way through the oxidation to improve uniformity. The oxidation rate for $Al_{0.98}Ga_{0.02}As$ is approximately 0.3 μm/min, and roughly twice faster than for $Al_{0.96}Ga_{0.04}As$.

4.2 Etching for intra-cavity phase tuning

Etching of semiconductors can be done using wet or dry etching. The most suitable technique depends on requirements of etch rate, selectivity, and anisotropy. Wet etching is intrinsically chemical and isotropic. For GaAs, wet etchants contain an oxidizer like H_2O_2 to oxidize the GaAs surface and an acid that dissolves the oxide. Since the etch rate of wet etching depends on the material composition and doping level, and with the etching being more isotropic, in this work dry etching with ions generated in a plasma and accelerated towards the sample by an electric field has been used for the intra-cavity phase tuning. The incident ions can be neutral or reactive for pure physical (sputtering) or chemical etching, or a combination thereof. Since a precise, stable, and reproducible etch rate, independent of material composition and doping, was needed we used pure physical etching with neutral ions. The technique used is Ar ion-beam etching in an Oxford Ionfab 300 Plus system equipped with an electron emitter for neutralizing the ion-beam and a rotating sample holder for uniform etching over large areas. The etch rate depends on the applied electric field (ion kinetic energy) and the ion beam current (ion density). In this work, the beam current was set to a low value of 3 mA while the Ar flow rate for both the beam and the neutralizer was set to 4 sccm. The voltage controlling the electric field was set to a low value of 300 V. The sample, which was rotated at 3 rpm during etching, was patterned with photoresist (positive photoresist AZ 1512) to enable measurements of etch depth using atomic force microscopy (AFM). The AFM tool (SPM-Bruker Dimension 1300) was also used for measurements of surface roughness.

4.3 Dielectric DBR deposition

In this work, the dielectric DBR was deposited using a sputtering technique. In sputtering, energetic atoms, Ar in this work, are generated in plasma and bombard a target. The Ar ion energy is high enough to overcome the binding energy of the target particles. As a result, these particles are sputtered away from the target and coat the surface of the sample. For conducting targets, DC sputtering is used where the target has a DC bias. Therefore, there is no accumulation of charge on the surface of the target. For insulating targets, RF sputtering is used. Reactive sputtering is used when thin films of compound materials are required. In reactive sputtering, a reactive gas is injected to the chamber and reacts with the particles of the target and form the thin film. The sputtering tool used in this work was an FHR MS 150. O_2 was used as the reactive gas to deposit SiO_2 and TiO_2. The O_2 flow was set to 15 sscm for SiO_2 and 4 sccm for TiO_2 and the Ar flow was set to 40 sccm for both films. Six pairs of SiO_2/TiO_2 were deposited one by one to build the dielectric DBR. The

thickness of each film was controlled by the deposition time. To minimize the errors in optical thickness, the physical thickness and refractive index of each layer were measured by ellipsometry before the deposition of the next layer. This was done by also depositing the layer on an adjacent Si wafer. If needed, additional material was deposited to reach the correct thickness.

4.4 Mode filter integration

The sub-wavelength grating mode filter was defined as the first step in the fabrication. Since the mode filter should be exactly at the center of the oxide aperture, electron beam lithography and metal alignment marks were used. The same alignment marks were also used to define the VCSEL mesa by electron beam lithography. Therefore, the mode filter and the oxide aperture were perfectly aligned. Dry etching was used to etch the grating into the top GaAs layer. Although a combination of reactive etching and physical sputtering could be used to form the sub-wavelength grating, Ar ion-milling was used for pure physical etching. Ar ion-milling provides the precise control of etch depth needed for the sub-wavelength grating.

Chapter 5

Future outlook

The project ultimately aims at demonstrating a monolithic multi-wavelength array of high-speed VCSELs in the wavelength range 1030-1070 nm. It is intended for flip-chip integration on a silicon photonics platform for multiplexing and fiber coupling. In terms of the VCSEL array, this requires a technique for precise wavelength setting of individual VCSELs in the array, a technique for transverse and polarization mode control, and a high-speed VCSEL design. Intra-cavity phase tuning was shown to enable the precision in wavelength setting needed (Paper A). Next, the technique will be used to demonstrate monolithic 4-channel multi-wavelength VCSEL arrays with precisely controlled wavelengths and channel spacing and with a minimum of variation of other parameters (e.g. threshold current and slope efficiency) across the channels. Thinning of the phase tuning layer and deposition of the dielectric DBR will be done early in the fabrication process to ensure a smooth interface to avoid additional optical cavity loss. The first generation of monolithic multi-wavelength VCSEL arrays will lack the transverse and polarization mode selectivity needed for integration on the silicon photonics platform and efficient coupling to the SiN waveguides. Therefore, the mode filter technique developed and successfully demonstrated for 850 nm VCSELs with a semiconductor top-DBR (Paper B) will be transferred to the VCSELs with a top dielectric DBR in the multi-wavelength VCSEL array. Finally, each VCSEL in the array should be able to operate at a baud-rate of 25 Gbaud/s under PAM-2 (25 Gbit/s) and PAM-4 (50 Gbit/s) modulation. This requires a high-speed design. Therefore, in addition to having a large intrinsic modulation bandwidth (high differential gain and optimum photon lifetime), the VCSELs will be designed for low resistance (an intra-cavity top-contact and graded composition interfaces and modulation doping in the bottom-DBR), low capacitance (multiple oxide layers), and low thermal impedance (high thermal conductivity bottom-DBR). To further reduce capacitance, a thick layer of benzocyclobutene (BCB) with a low dielectric constant will be used under the bond-pad.

Chapter 6

Summary of papers

Paper A

"Precise setting of micro-cavity resonance wavelength by dry etching" *Journal of Vacuum Science and Technology B*, vol. 37, 031217 (2019).

This paper presents a technique for precise setting of the resonance wavelength of VCSEL micro-resonators in a post-growth fabrication process. An accuracy of ±2 nm in the wavelength range 1040-1070 nm is achieved by intra-phase tuning using precise and stable Ar ion-beam etching. The precision in etching (±1 nm) limits the accuracy in wavelength setting to ±1 nm. The difference is caused by errors in the optical thickness (physical thickness and refractive index) of the dielectric layers used in the top-DBR and by the inherent non-uniformity of the epitaxial layer thicknesses. The technique is developed for the fabrication of monolithic multi-wavelength VCSEL arrays.

My contribution: I did all the fabrication, performed all measurements, and analyzed the results. I wrote the paper and presented the work at the 21st International Vacuum Congress 2019 (Malmö, Sweden).

Paper B

"High-power single transverse and polarization mode VCSEL for silicon photonics integration", *Optics Express* ,vol. 27, pp. 18892-18899, June 2019.

In this paper, a sub-wavelength grating mode filter was etched into the surface of an 850 nm VCSEL for selecting the fundamental transverse mode and pinning the polarization. A single transverse and polarization mode VCSEL with a record output power of 6.5 mW, >30 dB suppression of higher order transverse modes, >20 dB suppression of the orthogonal polarization mode, and narrow beam divergence of 10° (FWHM) is demonstrated. The VCSEL has the modal properties and output power required for light source integration on a silicon photonic integrated circuit.

My contributio: I performed all measurements and data analysis. I co-authored the paper.

References

[1] M. M. Group, "Internet World Stats," https://www.internetworldstats.com/stats.htm, accessed 2019-06-25, 2019.

[2] Cisco, "Cisco Global Cloud Index : Forecast and Methodology , 2014-2019," Tech. Rep., 2016. [Online]. Available: https://www.cisco.com/c/dam/en/us/solutions/collateral/service-provider/global-cloud-index-gci/white-paper-c11-738085.pdf

[3] N. Lehrer, "The largest data centers in the world," https://www.networkcomputing.com/cloud-infrastructure/the-largest-data-canters-in-the-world/d/d-id/1269250, accessed 2015-08-16, 2014.

[4] H. Menear, "Top 10 biggest data centres in the world," https://www.gigabitmagazine.com/top10/top-10-biggest-data-centres-world, accessed 2019-25-06, 2018.

[5] A. Larsson, "Advances in VCSELs for communication and sensing," *IEEE Journal of Selected Topics in Quantum Electronics*, vol. 17.

[6] O. Ueda and S. J. Pearton, *Materials and reliability handbook for semiconductor optical and electron devices.* Springer Science & Business Media, 2012.

[7] H. Blog, "Top of Rack Swith," https://fspro.hatenablog.com/entry/top-of-rack-switch, accessed 2019-27-06, 2018.

[8] X. Jin, F. Zhang, A. V. Vasilakos, and Z. Liu, "Green data centers: A survey, perspectives, and future directions," *arXiv preprint arXiv:1608.00687*, 2016.

[9] K. Bilal, S. U. R. Malik, O. Khalid, A. Hameed, E. Alvarez, V. Wijaysekara, R. Irfan, S. Shrestha, D. Dwivedy, M. Ali *et al.*, "A taxonomy and survey on green data center networks," *Future Generation Computer Systems*, vol. 36, pp. 189–208, 2014.

[10] M. Al-Fares, A. Loukissas, and A. Vahdat, "A scalable, commodity data center network architecture," in *ACM SIGCOMM Computer Communication Review*, vol. 38, no. 4. ACM, 2008, pp. 63–74.

[11] C. Kachris, K. Kanonakis, and I. Tomkos, "Optical interconnection networks in data centers: Recent trends and future challenges," *IEEE Communications Magazine*, vol. 51, no. 9, pp. 39–45, 2013.

[12] L. Wang, F. Zhang, J. A. Aroca, A. V. Vasilakos, K. Zheng, C. Hou, D. Li, and Z. Liu, "Greendcn: A general framework for achieving energy efficiency in data

center networks," *IEEE Journal on Selected Areas in Communications*, vol. 32, no. 1, pp. 4–15, 2013.

[13] A. Vahdat, H. Liu, X. Zhao, and C. Johnson, "The emerging optical data center," in *Optical Fiber Communication Conference*. Optical Society of America, 2011, p. OTuH2.

[14] G. Liu, J. Gao, H. Cheng, H.-C. Wu, E. Lau, L. Yuan, and C. Krause, "Thunderbolt interconnect–comparing optical and copper approaches," in *2017 IEEE International Symposium on Electromagnetic Compatibility & Signal/Power Integrity (EMCSI)*. IEEE, 2017, pp. 305–309.

[15] H. Cheng, J. Gao, H.-C. Wu, G. Liu, E. Lau, L. Yuan, and C. Krause, "Optics vs. copper, from the perspective of thunderbolt 3 interconnect technology," in *2016 China Semiconductor Technology International Conference (CSTIC)*. IEEE, 2016, pp. 1–3.

[16] M. Freebody, "Lasers evolve to meet the demands of optical communications," *Photonics spectra*, vol. 46, pp. 50–53, 02 2012.

[17] J. A. Tatum, D. Gazula, L. A. Graham, J. K. Guenter, R. H. Johnson, J. King, C. Kocot, G. D. Landry, I. Lyubomirsky, A. N. MacInnes *et al.*, "VCSEL-based interconnects for current and future data centers," *Journal of Lightwave Technology*, vol. 33, no. 4, pp. 727–732, 2015.

[18] P. Westbergh, E. P. Haglund, E. Haglund, R. Safaisini, J. Gustavsso, and A. Larsson, "High-speed 850 nm VCSELs operating error free up to 57 Gbit/s," *Electronics Letters*, vol. 49, no. 16, pp. 1021–1023, 2013.

[19] D. M. Kuchta, A. V. Rylyakov, F. E. Doany, C. L. Schow, J. E. Proesel, C. W. Baks, P. Westbergh, J. S. Gustavsson, and A. Larsson, "A 71 Gb/s NRZ modulated 850-nm VCSEL-based optical link," *IEEE Photonics Technology Letters*, vol. 27, no. 6, pp. 577–580, 2015.

[20] A. Larsson, E. Simpanen, J. Gustavsson, E. Haglund, E. Haglund, T. Lengyel, P. Andrekson, W. Sorin, S. Mathai, M. Tan *et al.*, "1060 nm VCSELs for long-reach optical interconnects," *Optical Fiber Technology*, vol. 44, pp. 36–42, 2018.

[21] M.-J. Li, "Novel optical fibers for data center applications," in *Broadband Access Communication Technologies X*, vol. 9772. International Society for Optics and Photonics, 2016, p. 977205.

[22] J. Lavrencik, S. Varughese, J. S. Gustavsson, E. Haglund, A. Larsson, and S. E. Ralph, "Error-free 100Gbps PAM-4 transmission over 100m wideband fiber using 850nm VCSELs," in *2017 European Conference on Optical Communication (ECOC)*. IEEE, 2017, pp. 1–3.

[23] P. Westbergh, J. S. Gustavsson, and A. Larsson, "VCSEL arrays for multicore fiber interconnects with an aggregate capacity of 240 Gb/s," *IEEE Photonics Technology Letters*, vol. 27, no. 3, pp. 296–299, 2014.

[24] I. Lyubomirsky, R. Motaghian, H. Daghighian, D. McMahon, S. Nelson, C. Kocot, J. Tatum, F. Achten, P. Sillard, D. Molin *et al.*, "100G SWDM4 transmission over 300m wideband MMF," in *2015 European Conference on Optical Communication (ECOC)*. IEEE, 2015, pp. 1–3.

[25] J. Lavrencik, S. Varughese, V. A. Thomas, G. Landry, Y. Sun, R. Shubochkin, K. Balemarthy, J. Tatum, and S. E. Ralph, "4$\lambda\times$ 100Gbps VCSEL PAM-4 transmission over 105m of wide band multimode fiber," in *Optical Fiber Communication Conference*. Optical Society of America, 2017, pp. Tu2B–6.

[26] J. Lavrencik, S. Varughese, V. A. Thomas, and S. E. Ralph, "Scaling VCSEL-MMF links to 1 Tb/s using short wavelength division multiplexing," *Journal of Lightwave Technology*, vol. 36, no. 18, pp. 4138–4145, 2018.

[27] H. Hatakeyama, T. Anan, T. Akagawa, K. Fukatsu, N. Suzuki, K. Tokutome, and M. Tsuji, "Highly reliable high-speed 1.1 μ m-range VCSELs with InGaAs/GaAsP-MQWs," *IEEE Journal of Quantum Electronics*, vol. 46, no. 6, pp. 890–897, 2010.

[28] S. Sweeney, A. Phillips, A. Adams, E. O'reilly, and P. Thijs, "The effect of temperature dependent processes on the performance of 1.5-μm compressively strained InGaAs (P) MQW semiconductor diode lasers," *IEEE Photonics Technology Letters*, vol. 10, no. 8, pp. 1076–1078, 1998.

[29] R. E. Freund, C.-A. Bunge, N. N. Ledentsov, D. Molin, and C. Caspar, "High-speed transmission in multimode fibers," *Journal of Lightwave Technology*, vol. 28, no. 4, pp. 569–586, 2009.

[30] J. A. Kash, A. F. Benner, F. E. Doany, D. M. Kuchta, B. G. Lee, P. K. Pepeljugoski, L. Schares, C. L. Schow, and M. Taubenblatt, "Optical interconnects in exascale supercomputers," in *2010 23rd Annual Meeting of the IEEE Photonics Society*. IEEE, 2010, pp. 483–484.

[31] C. Minkenberg, "HPC networks: Challenges and the role of optics," in *2015 Optical Fiber Communications Conference and Exhibition (OFC)*. IEEE, 2015, pp. 1–3.

[32] C. J. Chang-Hasnain, M. W. Maeda, J. P. Harbison, L. Florez, and C. Lin, "Monolithic multiple wavelength surface emitting laser arrays," *Journal of lightwave technology*, vol. 9, no. 12, pp. 1665–1673, 1991.

[33] M. Arai, T. Kondo, A. Onomura, A. Matsutani, T. Miyamoto, and F. Koyama, "Multiple-wavelength GaInAs-GaAs vertical cavity surface emitting laser array with extended wavelength span," *IEEE Journal of selected topics in quantum electronics*, vol. 9, no. 5, pp. 1367–1373, 2003.

[34] J. Geske, D. Leonard, M. H. MacDougal, B. Barnes, and J. E. Bowers, "CWDM vertical-cavity surface-emitting laser array spanning 140 nm of the C, S, and L fiber transmission bands," *IEEE Photonics Technology Letters*, vol. 16, no. 5, pp. 1227–1229, 2004.

[35] A. Fiore, Y. Akulova, J. Ko, E. Hegblom, and L. A. Coldren, "Postgrowth tuning of semiconductor vertical cavities for multiple-wavelength laser arrays," *IEEE journal of quantum electronics*, vol. 35, no. 4, pp. 616–623, 1999.

[36] D. Huffaker and D. Deppe, "Multiwavelength, densely-packed 2 $\times$ 2 vertical-cavity surface-emitting laser array fabricated using selective oxidation," *IEEE Photonics Technology Letters*, vol. 8, no. 7, pp. 858–860, 1996.

[37] E. Haglund, J. S. Gustavsson, J. Bengtsson, Å. Haglund, A. Larsson, D. Fattal, W. Sorin, and M. Tan, "Demonstration of post-growth wavelength setting of VCSELs using high-contrast gratings," *Optics express*, vol. 24, no. 3, pp. 1999–2005, 2016.

[38] T. Wipiejewski, M. Peters, E. Hegblom, and L. Coldren, "Vertical-cavity surface-emitting laser diodes with post-growth wavelength adjustment," *IEEE photonics technology letters*, vol. 7, no. 7, pp. 727–729, 1995.

[39] S.-Y. Hu, J. Ko, and L. A. Coldren, "High-performance densely packed vertical-cavity photonic integrated emitter arrays for direct-coupled WDM applications," *IEEE Photonics Technology Letters*, vol. 10, no. 6, pp. 766–768, 1998.

[40] J.-H. Shin and B.-S. Yoo, "Fabrication method for multiple wavelength vertical-cavity emitter arrays by SiN_x layer thickness control," *IEEE Photonics Technology Letters*, vol. 11, no. 5, pp. 509–511, 1999.

[41] P. B. Dayal, T. Sakaguchi, A. Matsutani, and F. Koyama, "Multiple-wavelength vertical-cavity surface-emitting lasers by grading a spacer layer for short-reach wavelength division multiplexing applications," *Applied physics express*, vol. 2, no. 9, p. 092501, 2009.

[42] R. Suzuki, H. Motomura, and S. Satoh, "Vertical cavity surface emitting lasers with precise multi-wavelength control," in *2016 International Semiconductor Laser Conference (ISLC)*. IEEE, 2016, pp. 1–2.

[43] Y. Kawakita, K. Takaki, M. Funabashi, S. Imai, and A. Kasukawa, "1060nm single-mode multi-wavelength VCSEL array with intra-cavity phase tuning layers," in *2014 International Semiconductor Laser Conference*. IEEE, 2014, pp. 207–208.

[44] S. Spiga, C. Xie, P. Dong, M.-C. Amann, and P. Winzer, "Ultra-high-bandwidth monolithic VCSEL arrays for high-speed metro networks," in *2014 16th International Conference on Transparent Optical Networks (ICTON)*. IEEE, 2014, pp. 1–4.

[45] C. Xie, S. Spiga, P. Dong, P. Winzer, M. Bergmann, B. Kögel, C. Neumeyr, and M.-C. Amann, "400 Gb/s PDM-4PAM WDM system using a monolithic 2×4 VCSEL array and coherent detection," *Journal of Lightwave Technology*, vol. 33, no. 3, pp. 670–677, 2014.

[46] D. Dai, Z. Wang, J. F. Bauters, M.-C. Tien, M. J. Heck, D. J. Blumenthal, and J. E. Bowers, "Low-loss Si_3N_4 arrayed-waveguide grating (de) multiplexer using nano-core optical waveguides," *Optics express*, vol. 19, no. 15, pp. 14 130–14 136, 2011.

[47] H. Lu, J. S. Lee, Y. Zhao, C. Scarcella, P. Cardile, A. Daly, M. Ortsiefer, L. Carroll, and P. OâBrien, "Flip-chip integration of tilted VCSELs onto a silicon photonic integrated circuit," *Optics express*, vol. 24, no. 15, pp. 16 258–16 266, 2016.

[48] H. Lu, J. S. Lee, Y. Zhao, P. Cardile, A. Daly, L. Carroll, and P. O'Brien, "Hybrid integration of VCSELs onto a silicon photonic platform for biosensing application," in *Optical Diagnostics and Sensing XVII: Toward Point-of-Care Diagnostics*, vol. 10072. International Society for Optics and Photonics, 2017, p. 100720K.

[49] A. Haglund, J. S. Gustavsson, J. Vukusic, P. Modh, and A. Larsson, "Single fundamental-mode output power exceeding 6 mw from VCSELs with a shallow surface relief," *IEEE Photonics Technology Letters*, vol. 16, no. 2, pp. 368–370, 2004.

[50] H. Martinsson, J. Vukusic, and A. Larsson, "Single-mode power dependence on surface relief size for mode-stabilized oxide-confined vertical-cavity surface-emitting lasers," *IEEE Photonics Technology Letters*, vol. 12, no. 9, pp. 1129–1131, 2000.

[51] A. Haglund, J. S. Gustavsson, J. Bengtsson, P. Jedrasik, and A. Larsson, "Design and evaluation of fundamental-mode and polarization-stabilized VCSELs with a subwavelength surface grating," *IEEE journal of quantum electronics*, vol. 42, no. 3, pp. 231–240, 2006.

[52] L. A. Coldren, S. W. Corzine, and M. L. Mashanovitch, *Diode lasers and photonic integrated circuits*. John Wiley & Sons, 2012, vol. 218.

[53] Y. Satuby and M. Orenstein, "Mode-coupling effects on the small-signal modulation of multitransverse-mode vertical-cavity semiconductor lasers," *IEEE journal of quantum electronics*, vol. 35, no. 6, pp. 944–954, 1999.

[54] R. Michalzik, *VCSELs: fundamentals, technology and applications of vertical-cavity surface-emitting lasers*. Springer, 2012, vol. 166.

[55] K. Takaki, "A recoded 62% PCE and low series and thermal resistance VCSEL with a double intra-cavity structure," in *IEEE International Semiconductor Laser Conf., Sept. 2008*, 2008.

[56] N. Nishiyama, M. Arai, S. Shinada, K. Suzuki, F. Koyama, and K. Iga, "Multi-oxide layer structure for single-mode operation in vertical-cavity surface-emitting lasers," *IEEE Photonics Technology Letters*, vol. 12, no. 6, pp. 606–608, 2000.

[57] Y. Chang, C. Wang, L. Johansson, and L. Coldren, "High-efficiency, high-speed VCSELs with deep oxidation layers," *Electronics Letters*, vol. 42, no. 22, pp. 1281–1282, 2006.

[58] S. Adachi, "Lattice thermal resistivity of III–V compound alloys," *Journal of Applied Physics*, vol. 54, no. 4, pp. 1844–1848, 1983.

[59] E. Simpanen, J. Gustavsson, E. Haglund, E. Haglund, A. Larsson, W. Sorin, S. Mathai, and M. Tan, "1060 nm single-mode vertical-cavity surface-emitting laser operating at 50 Gbit/s data rate," *Electronics Letters*, vol. 53, no. 13, pp. 869–871, 2017.

[60] J. S. Gustavsson, Å. Haglund, J. A. Vukušić, J. Bengtsson, P. Jedrasik, and A. Larsson, "Efficient and individually controllable mechanisms for mode and polarization selection in VCSELs, based on a common, localized, sub-wavelength surface grating," *Optics express*, vol. 13, no. 17, pp. 6626–6634, 2005.